# THEORETICAL AND EXPERIMENTAL STUDY OF A SINGLE-PASS SOLAR AIR COLLECTOR FOR DRYING FOOD PRODUCTS

***Abdelouahab BOUBEGHAL [*1], Salim AOUALMIT [1] , Abla CHAKER [2] , Ahmed MEDIANI [3], Mohamed walid AZIZI [1]***

[1]Department of Mechanical and Electromechanical, University Centre Abdelhafid Boussouf Mila, Algeria

[2]Laboratory of Energy Physics, Faculty of Exact Sciences University Constantine, 25000 Constantine, Algeria

[3]Research Unit for Renewable Energies in Saharan region (URER-MS), Adrar, Algeria

[*] Corresponding author; E-mail: a.boubeghal@centre-univ-mila.dz

*This paper involved a theoretical and experimental study of a single-pass solar air collector to supply hot air to a solar dryer. A Fortran code is developed to solve the heat transfer equations and determine the thermal performance of the collector's components, such as the absorber plate, glass cover, and heat transfer air. Three similar solar collectors, installed at different inclination angles (horizontal, 30° inclination, and 70° inclination), were constructed and tested at the Research Unit (URER-MS) in southern Algeria. The effect of the collector's inclination on its thermal performance has been investigated. The results show that the collector's performance is strongly influenced by the inclination angle, with the optimal angle varying according to seasonal conditions. The model validation revealed percentage deviations between theoretical and experimental results across all tested inclination angles as follows: absorber temperature (4.8– 10%), heated air temperature (5.2– 14.8 %), glass cover temperature (10.7 – 17.3 %), and ambient temperature (5.4– 6.4%). These deviation ranges confirm the reasonable accuracy of the theoretical model in predicting system performance under varying operational conditions.*

Keywords: *Solar air collector, Thermal performance, Experimental, Numerical simulation, Inclination angle*

## 1. Introduction

Solar air collectors represent a promising technology for the efficient and sustainable use of solar energy. Their ability to convert sunlight into useful heat for various applications, particularly in drying agricultural products, makes them an attractive solution for producers and industries looking to enhance their processes' sustainability and thermal efficiency [1]. Solar air collectors face two key challenges: low air thermal capacity and a heat transfer coefficient between the air and the absorber, which require careful design and compensation. With the progress of numerical methodologies, computing technology, and hardware, advanced mathematical models have become essential tools for in-depth studies of solar air collectors [2]. These models offer highly cost-effective solutions, enabling the generation of extensive

datasets and facilitating efficient parametric analyses to optimize system performance [3]. Furthermore, numerical simulations are particularly advantageous for examining parameters that are challenging to test experimentally, significantly reducing both the financial burden and the time required for physical experimentation [4, 5]. Also, they can be utilized study the effects of different characteristics of the thermal system [6].

The use of flat-plate solar air collectors (SACs) to supply hot air to agricultural product dryers has become a common technique in recent years, owing to the significant energy requirements of the drying process and the rising costs associated with it. To successfully conduct such an operation, it is essential to integrate a suitable collector into the drying chamber, whose operating temperatures enable achieving a reduced drying time and a high-quality dry product [7-11]. The principal types of SACs are: the single pass; with air flow below or above the absorber and double pass; with air flow below and above the absorber.

Over the years, a number of SACs designs have been designed, tested, and proposed. The flat plate type is the most widely used form due to its ease of construction using inexpensive, locally available materials [12-15]. In order to simulate the collector's behavior under different climate conditions and latitudes, computational modeling is crucial [16, 17]. Chabane et al., [18] examined the influence of rectangular baffles on the thermal performance of a solar air collector. The experiments were conducted in south Algeria (altitude of 34°) over several days. The study involved varying the collector's inclination angle from $\beta = 0°$ to $\beta = 55°$. The results show a small effect for the angle of inclination of the collector on the pressure drop because the latter is mainly affected by the flow, not by gravity. Roman and Hensel [19] compared steady-state and transient solar air heater models. While steady-state worked well in clear skies, it missed large temperature swings during clouds due to rapid solar changes. The transient model, using minute-by-minute weather data, captured these variations with deviations up to 15°C. This shows transient models are vital for precise short-term predictions in solar drying and heat storage. Hernández and Salvo [20] conducted a parametric analysis using computational modeling to compare the thermal performance of two air-heating solar collector configurations. For two inclinations relevant to building thermal conditioning applications, the study evaluated the dependence of daily thermal efficiency on factors such as the circulating air flow rate, and the collection area. The collector is inclined at an angle of 35°(latitude +10°) has a 3% higher value than the vertical slope during winter due to the daily thermal efficiency dependence on the slope. Mutar et al., [21] developed a single-pass solar collector and evaluated its performance under the climatic conditions of Al Ramadi, Iraq. The study investigates and compares three absorber plate configurations with and without metal foam (MF). The results indicate that, in winter, using MF fins with a 45° inclination angle results in a greater air temperature differential than both MF fins at 0°. Selmi et al., [22] used a plate solar collector on steel with a covered area of 2 m² to conduct the experiments. The tests were carried out under natural convection airflow. It was found that natural convection provided better collector performance than forced convection. Suresh et al., [23] studied a forced solar dryer with a single-pass solar air collector using a galvanized iron absorber plate and Polyethylene foam insulation. The average air outlet temperature difference was 19.7 K, with solar radiation at 817.33 W/m². The drop in temperature was due to decreased solar radiation, leading to heat loss in the collector. In addition, the increased airflow rate reduced collector efficiency. Al Kayem et al., [24] analyzed the optimal inclination angle for the combined absorption-convection heat transfer mechanism. The results show the transient behavior of the solar air heater by analyzing the Nusselt number (Nu) over time at inclination angles of 30°, 50°, and 70°. The most increased Nu is observed at

50°, followed by 30° and 70°. The impact of inclination on heat transfer can clarify this tendency. A lower inclination improves solar irradiance absorption; it is less practical for heat transfer. On the other hand, at higher inclination angles, such as 70°, the absorber plate is less susceptible to direct solar irradiance, reducing solar insolation.

Predicting system behavior throughout the year is essential for a more comprehensive evaluation. However, most studies are confined to specific periods, limiting their applicability. In addition, as we know, previous investigations on the performance of solar collectors used a single prototype, which led to inaccurate comparisons due to potential interpretations of climatic conditions from day to day.

This study also aims to develop a simplified yet accurate mathematical model to simulate the thermal performance of the solar collector. The model will predict key operational parameters, including temperature distributions across critical components (absorber plate, glass cover, and airflow) and dynamic external conditions such as ambient temperature and solar irradiance intensity.

## 2. Methodology

### 2.1. Description of solar collector

The authors constructed a solar collector measuring 2 m in length and 1 m in width, which is a single-pass air collector with natural convection airflow above the absorber. The frame of the solar collector is constructed from galvanized iron, while the support structure consists of square steel tubes. The solar collector consists of an absorber plate, a cover glass, and a thermally insulated base. The absorber plate is chosen to be in a galvanized iron (GS) sheet for its great specific heat capacity and its high thermal conductivity. The GS sheet is painted black to absorb much sun radiation and minimize heat losses inside the collector. The absorber is isolated by foam to decrease heat losses to the surroundings. Due to its low thermal conductivity, we used insolation foam as the basis for thermal insulation. We chose the cover on Polycarbonate to allow the entire solar spectrum to reach the absorber. The incoming solar radiation passes through the glass cover, which is 45 mm above the absorber.

**Table 1. Material and properties in components of a solar air collector**

| Properties | Absorber ( Galvanized iron) | Glass cover (Polycarbonate) | Insolation (Foam) | Airflow |
|---|---|---|---|---|
| Thermal conductivity ( $W\ m^{-1}\ K^{-1}$) | 80 | 1.05 | 0.03 | 0.02735 |
| Density ($kg\ m^{-3}$) | 7850 | 1200 | 30 | 1.1774 |
| Specific heat ($J\ kg^{-1}\ K^{-1}$) | 450 | 1226 | 1764 | 1700 |
| Thickness (m) | 0.002 | 0.003 | 0.05 | - |
| Absorptance | 0.95 | - | - | - |
| Transmittance | - | 0.8 | - | - |
| Emittance | 0.95 | 0.9 | - | - |
| Specific air mass flow rate ( $kg\ s^{-1}m^{-2}$) | - | - | - | 0.015 |

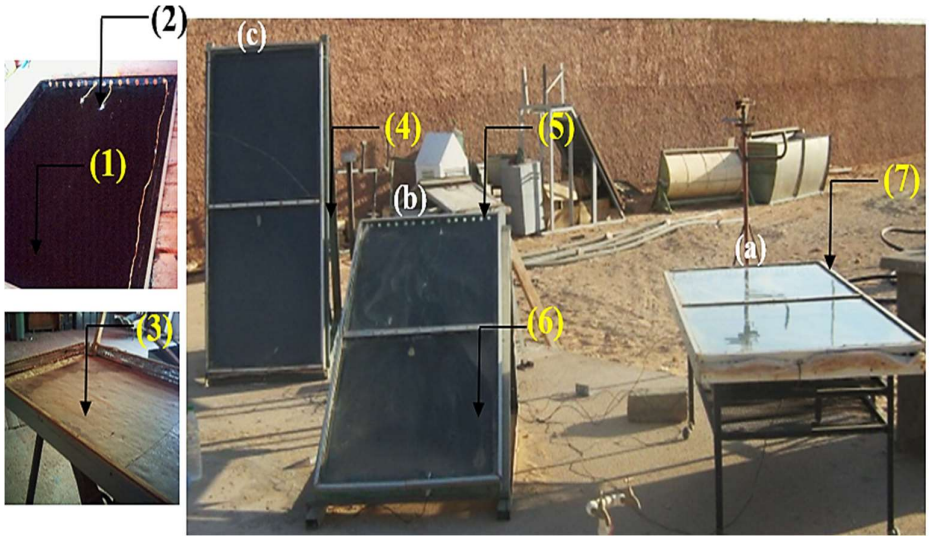


(1) Absorber plate, (2) Thermocouple connecter, (3) Insolation, (4) Support, (5) Air orifice (6) Glass cover, (7) Farme

**Figure 1. Three similar solar collectors for three inclinations: (a) Horizontal, (b) Inclination 30°, and (c) Inclination 70°**

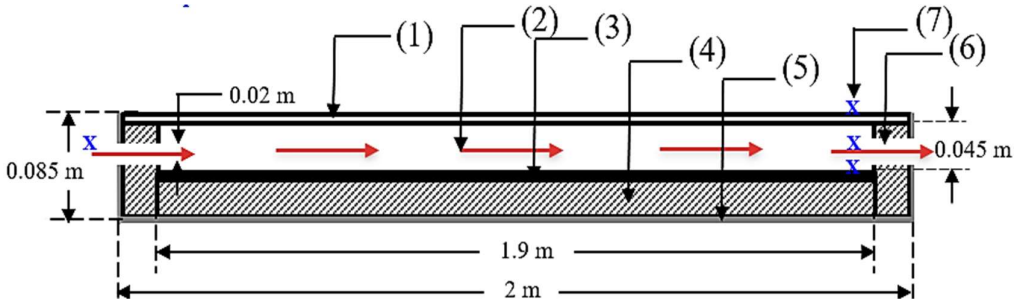


(1) Glass cover, (2) Natural air flow, (3) Absorber plate, (4) Insolation, (5) Farme, (6) Air orifice, (7) Thermocouples connecter

**Figure 2. Schematic view of the solar air collector**

### 2.2. Measuring instrumentations

- A calibrated thermocouples type K (Chromel-Alumel; 0.2mm diameter; ±0.1°C resolution; ±2% uncertainty; -50 to 1000°C range) have been used to measure the temperature at different locations for each collector, including the air ambient temperature and outlet temperature at the outlet of collector, as well as the glass cover and absorber temperatures at the center. The ambient air temperature was measured near the air intake openings of the solar collector.
- Pyranometers type Kipp & Zonen CMP11 has a measurement range of 0 to 1500 W/m², ±5% uncertainty, sensitivity of 7 to 14 µV/W/m², and a resolution of ±1 W/m². It measured global solar irradiance on a 30° inclined plane.
- The Hydra Datalogger 2620A (±0.018% uncertainty, 20-channel scanning, and 256 KB memory) was used to record data from a pyranometer and Type K thermocouples in our collector. It offers a resolution of 0.001 mV for voltage reading and 0.1°C for Type K thermocouples. Its multiple input

channels and data logging capabilities enable continuous system monitoring, while the RS-232 interface ensures easy data transfer for analysis.

## 2.3. Experimental

We conducted a series of experiments at the Research Unit on Renewable Energies in Saharan Environment (URER-MS) in Adrar, south Algeria, where the latitude is 27.88° N and longitude is -0.297° W. During the experiments, three similar collectors were positioned facing south to maximize their exposure to the highest solar radiation intensity. A measurement campaign was conducted on April 20, 2024. At the same time, the collectors were tested at various inclinations (horizontal, 30° inclination, and 70° inclination). The measurements were automatically recorded every 10 minutes using a data acquisition device, starting at 7:00 AM and continuing until 8:00 AM the following day. During each measurement, the following parameters were recorded: solar radiation, absorber plate temperature, glass cover temperature, outlet air temperature, and ambient temperature.

## 2.4. Mathematical modeling

We employed the global method to model our solar air collector, as outlined by Duffie and Beckman [25]. This method provides an efficient framework for calculating the system's thermal performance by balancing the incoming solar irradiance, heat losses, and heat gained by the air. Using relatively simple equations to predict the air temperature increase when passing through the collector. The mathematical model is established on the one-dimensional transient heat equation, devoted to the three primary elements of the system: the glass cover, absorber plate, and the air. In this model, the temperature gradient is considered to exist only along the main flow direction, while the air velocity is considered uniform across the width of the collector.

### *2.4.1. Simplifying assumptions*

The numerical modeling methodology developed in this investigation incorporates several critical hypotheses that have been assumed based on specified methodologies [19], [25]:

- The Global approach considers steady-state requirements, suggesting that the collector's performance is examined at a constant time interval without modifications in energy storage,
- The properties of the air (like mass flow rate and specific heat) are assumed to be constant during the process,
- The materials' physical characteristics remain constant within the collector's temperature range.
- The variations in the thermal inertia of the collector components over time can be considered negligible ($mCp\ dT/dt \approx 0$) because the total mass and thermal capacity of the components are relatively small,
- The solar air collector's side thermal losses are considered negligible,
- The heat loss resistance through the back of the collector is attributed solely to the insulation material, as the contributions of radiation and wind are negligible.

### *2.4.2. Heat balance*

To calculate the thermal performance of the collector, we applied the energy balance for developing a mathematical model for each component as follows:

- At the surface of the glass covers

$$hc_{f-v}(T_f - T_v) + hr_{b-v}(T_b - T_v) - U_t(T_v - T_a) = 0 \quad (1)$$

- At the absorber plate

$$(\tau_v\ \alpha_b)G - U_b(T_b - T_a) - hr_{b-v}(T_b - T_v) - hc_f(T_b - T_f) = 0 \quad (2)$$

- At flowing air between glass cover and absorber

$$\frac{\dot{m}_f\, Cp_f}{w}.\frac{dT_f}{dx} = hc_f(T_b - T_f) + hc_f(T_v - T_f) \quad (3)$$

In the above equations (1) to (3), *G* refers to solar irradiance, *T* to temperature, *x* to the position along the collector length, $\tau$ to solar transmittance, $\alpha$ to solar absorptance, and *w* to the width of the collector. The different heat transfer coefficients are referred to by *h*, with subscripts *c* and *r* referring to natural convection and radiation modes. Subscripts *b* and *v* refer to the main collector elements, namely the absorber plate and glass cover. Subscripts *a* and $f$ refer to the ambient air and the flowing air, respectively. The specific heat capacity and mass flow rate of the flowing air are denoted by and, respectively. The variable *Ut* refers to the wind convection coefficient, while *Ub* represents the back heat loss coefficient.

By eliminating $T_b$ and $T_v$ the equation (3) becomes [26]:

$$\dot{m}_f\ Cp_f \frac{dT_f}{dx} = w.F'.\{G(\tau_v\alpha_b) - U_L(T_f - T_a)\} \quad (4)$$

With:

$$F' = \frac{2hc_f\ hr_{b-v}+hc_f U_t+hc_f^2}{(U_b+hc_f+hr_{b-v})(U_t+hc_f+hr_{b-v})-hr_{b-v}^2} \quad (5)$$

$$U_L = \frac{(U_b+U_t)\left(2hc_f hr_{b-v}+hc_f^2\right)+2\ U_t\ U_b\ hc_f}{2hc_f\ hr_{b-v}+hc_f U_b+hc_f^2} \quad (6)$$

F': is a dimensionless number which characterizes the thermal efficiency factor of the collector.

$U_L$: is the overall thermal loss coefficient of the collector and is expressed in $Wm^{-2}K^{-1}$

The first-order nonlinear differential equation (4) is governed by the following boundary condition:

$$T_f(x = 0) = T_{fe} \quad (7)$$

Assuming that F′ and $U_L$ are independent of the position x, the solution of the differential equation (4) is [27]:

$$\frac{(T_f(x) - T_a)-\left(\frac{(\tau_v\ \alpha_b)G}{U_L}\right)}{(T_{fe}- T_a)-\left(\frac{(\tau_v\ \alpha_b)G}{U_L}\right)} = exp\left(-\frac{w.F'.U_L}{\dot{m}_f.Cp_f}.x\right) \quad (8)$$

For a collector (length L), the outlet fluid temperature $T_{fe}$ is found by substituting L for *x* in (8):

$$\frac{(T_f - T_a)-\left(\frac{(\tau_v\ \alpha_b)G}{U_L}\right)}{(T_{fe} - T_a)-\left(\frac{(\tau_v\ \alpha_b)G}{U_L}\right)} = exp\left(-\frac{w\ F'\ U_L}{\dot{m}_f\ Cp_f}\ L\right) \quad (9)$$

*a) Coefficient of convective heat transfer*

The coefficient of convective transfer between glass cover and ambient environment is expressed [25]:

$$U_t = 5.67 + 3.86\ v_{ext} \quad (10)$$

The coefficient of convective transfer between air flow and collector walls, which are absorber and glass cover, is calculated by [27]:

$$hc_f = \frac{Nu\,\lambda}{D_H} \quad (11)$$

where $Nu$ is Nusselt number, $D_H$ is the hydraulic diameter and λ is the thermal conductivity of air.
To calculate the Nusselt number, the correlations that follow are used [19]:
Laminar flow (Re < 2100)

$$\text{Gz} < 100 : Nu = 3.66 + 0.085\, Gz/\left(1 + 0{,}047\, Gz^{2/3}\right) \quad (12)$$

$$\text{Gz} > 100 : Nu = 0.186\, Gz^{1/3} + 0.87\left(1 + 0.015\, Gz^{1/3}\right) \quad (13)$$

Transitional flow ($2100 < \text{Re} < 10^4$)

$$Nu = 0.166\left(Re^{2/3} - 125\right)Pr^{1/3}\left(1 + \left(\frac{D}{L}\right)^{2/3}\right) \quad (14)$$

Turbulent flow ($\text{Re} > 10^4$)

$$Nu = 0.023\, Re^{0,8}\, Pr^{0,33} \quad (15)$$

Where $Pr$ is Prandtl number, $Re$ is Reynolds number and $Gz$ is Graetz number
The Prandtl number, Reynolds number and Graetz number are expressed respectively [25:

$$Pr = \frac{\mu_a}{\lambda_a}\, Cp_a \quad (16)$$

$$Re = \frac{\rho_a}{\mu_a}\, D\, v_a \quad (17)$$

$$Gz = Re\,\text{Pr}\left(\frac{D}{L}\right) \quad (18)$$

*b) Coefficient of radiative heat transfer*

The coefficient of radiative transfer between the glass cover and the absorber is given by [27]:

$$hr_{b-v} = \sigma \frac{(T_b + T_v).(T_b^2 + T_v^2)}{\frac{1}{\varepsilon_b} + \frac{1}{\varepsilon_v} - 1} \quad (19)$$

*c) Coefficient of heat loss of the back*

The loss coefficient through the back of the solar air collector is given by [19], [28]:

$$U_b = \frac{k_i}{e_i} \quad (20)$$

Where $e_i$ and $k_i$ are the thickness of the insulation material and the thermal conductivity respectively.

*d) Solar irradiance*

In the Liu & Jordan model, global irradiance is the sum of direct, diffuse, and reflected solar irradiance. This relationship is given by the expression [25], [28]:

$$G = G_{bh}R_b + \frac{G_{dh}(1+cos\ )}{2} + G_r \quad (21)$$

Where: $R_b$ is the inclination factor for direct solar irradiance and is given by the following equation:

$$R_b = \frac{\cos(h-\beta)*\cos(\delta)*\cos(\omega)+\sin(h-\beta)*\sin(\delta)}{\cos(h)*\cos(\delta)*\cos(\omega)+\text{si}\ \ (h)*\sin(\delta)} \quad (22)$$

Where : $\omega$ is the hour angle, $\beta$ is the inclination, $\delta$ is the declination and $h$ is the solar altitude.
The reflected solar irradiance is given by the following equation :

$$G_r = a(G_{bh} + G_{dh})\left(\frac{1-\cos\beta}{2}\right)\tau \quad (23)$$

The diffuse solar irradiance received on a horizontal surface is given by the following equation:

$$G_{dh} = G_c(0.2710 - 0.2939\,\tau)\,sinh \tag{24}$$

The direct solar irradiance received on a horizontal surface can be expressed as:

$$G_{bh} = G_c\,\tau\,sinh \tag{25}$$

Where $\tau$ is atmospheric transmittance factor for direct beam irradiance and $G_c$ is extraterrestrial solar irradiance at the top of the atmosphere (W/m²).

$$G_c = G_0\left[1 + 0.033\,cos\left(\frac{360}{365}\right)n\right] \tag{26}$$

Where $G_0$ is solar constant (approximately 1361 W/m²) and n is day of the year

*e) Ambient temperature*

The ambient temperature is calculated using the formula [25]:

$$T_a = \frac{T_{max}+T_{min}}{2} + \frac{T_{max}-T_{min}}{2}\sin\left[(t - t_{max})\frac{\pi}{12}\right] \tag{27}$$

Where:

$T_{max}$ and $T_{min}$ represent the maximum and minimum ambient temperatures during a day.

$t$ is current time (hour) and $t_{max}$ is time of maximum temperature.

### *2.4.3. Solution procedure*

An iterative procedure accounts for the temperature dependence on the heat transfer coefficients, ensuring more accurate modeling. The coefficients are first initialized using standard formulas using initial temperatures corresponding to sunrise, and then the equations are solved assuming that these coefficients are constant. Successive iterations refine the results by updating the coefficients with new temperatures. The process is repeated until convergence is ensured. The flow chart illustrates the numerical solution presented in Fig. 3.

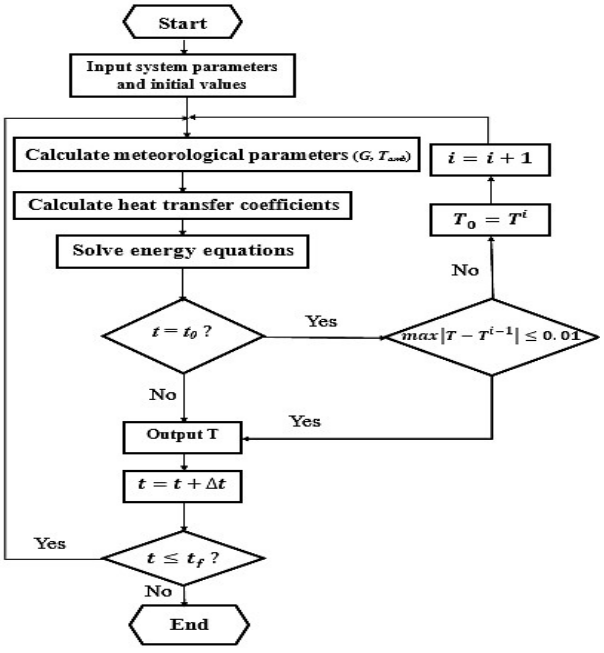


**Figure 3. Flow chart of numerical solution**

At the initial time, corresponding to sunrise, the absorber, glass cover, and inlet air temperatures are assumed to equal the ambient temperature. To cover the entire day, we initialize the temperatures with a step of 1 min each time.

## 3. Results

### 3.1. Thermal behaviour of the solar flat collector

Fig. 4 shows the temporal variation of the simulated absorber temperatures, glass cover, heated air, and ambient air throughout the four days representing each year's season (January 20, April 20, July 20, October 20) closely conforms to a cloche-shaped. The maximum values occur at 1:00 PM, with the highest value recorded on July 20.

We observe that the maximum values of the heated air at the outlet are remarkably higher than the maximum ambient temperatures recorded during these days (Tab. 2). Based on these results, the important distinction between the air inlet temperature (ambient) and the air outlet temperature is primarily due to the temperature gradient between the absorber and the air inlet, which conducts higher heat transfer.

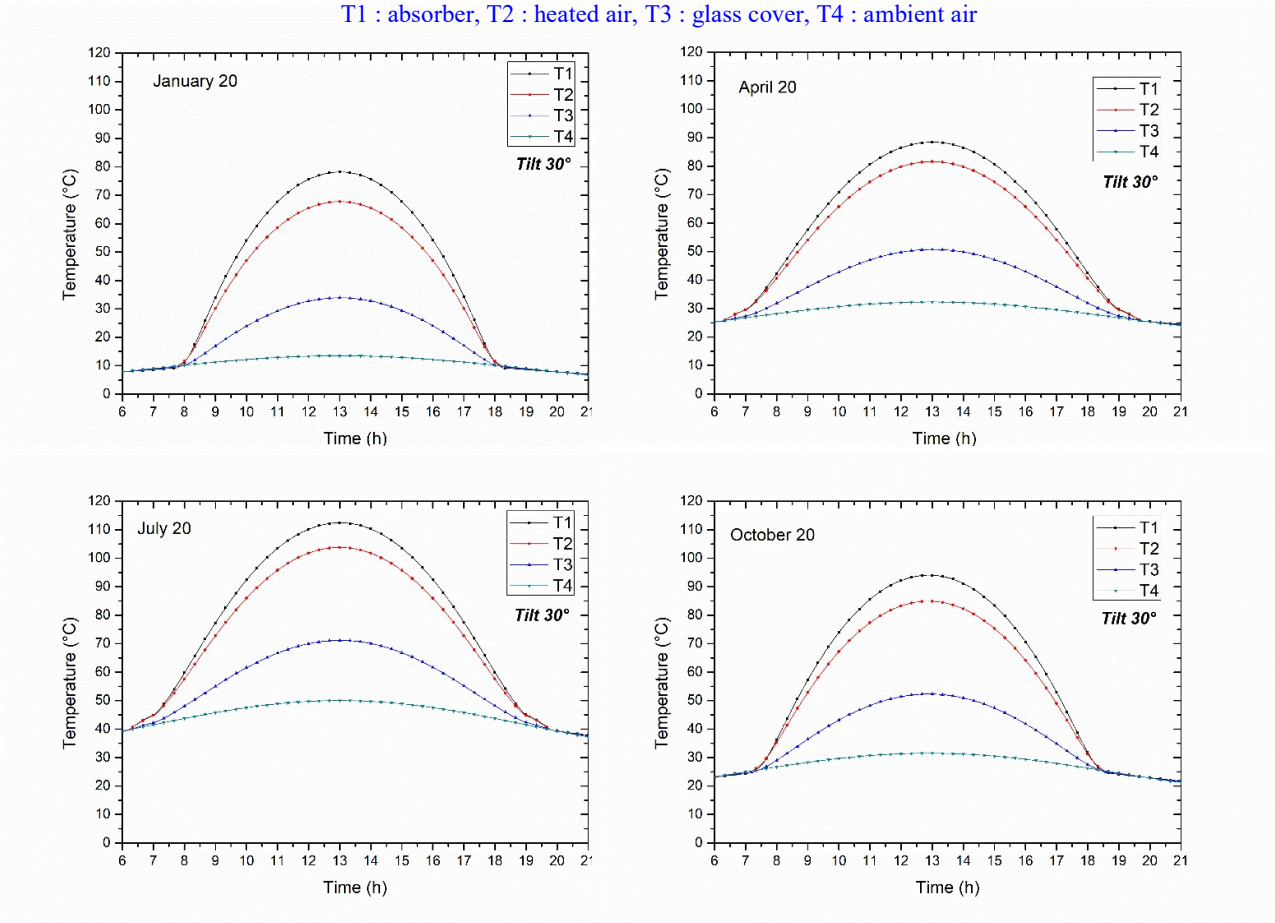


**Figure 4. Temporal variation of simulated collector component temperatures on different days: (a) January 20, (b) April 20, (c) July 20, (d) October 20**

**Table 2. Simulated maximum temperature values of heat air**

| | January 20 | April 20 | July 20 | October 20 |
|---|---|---|---|---|
| $T_f$ (°C) | 68 | 82 | 104 | 85 |
| $\Delta$ ($T_f - T_{amb}$) (°C) | 54 | 50 | 56 | 53 |

### 3.2. Effect of collector inclination

#### *3.2.1. Solar irradiance*

Fig. 5 compares daily solar irradiance intensity for different solar collector inclinations in winter and summer. The simulated results indicate that solar irradiance is weak in the morning and increases until it reaches the peak at noon, then decreases and reaches the minimum value at sunset. In winter, solar irradiance on a horizontal plane is relatively weak. At the same time, it becomes more intense on inclined planes (Fig. 5a). On the contrary, Fig. 5b shows that in summer, the intensity of solar irradiance is weak for the 70° inclined plane but higher for both the horizontal and 30° inclined plane. This phenomenon occurs because of seasonal variations in the sun's position relative to the Earth. Solar radiation strikes the surface in summer at nearly perpendicular angles, while in winter, the incident angle becomes much more oblique. Consequently, to optimize solar energy capture, the collector's tilt angle should be adjusted seasonally at a shallower angle in summer to align with the high sun position and at a steeper angle in winter to better intercept the lower-angled sunlight. Additionally, this angle reduces reflection losses and increases the solar irradiance the collector captures [28].

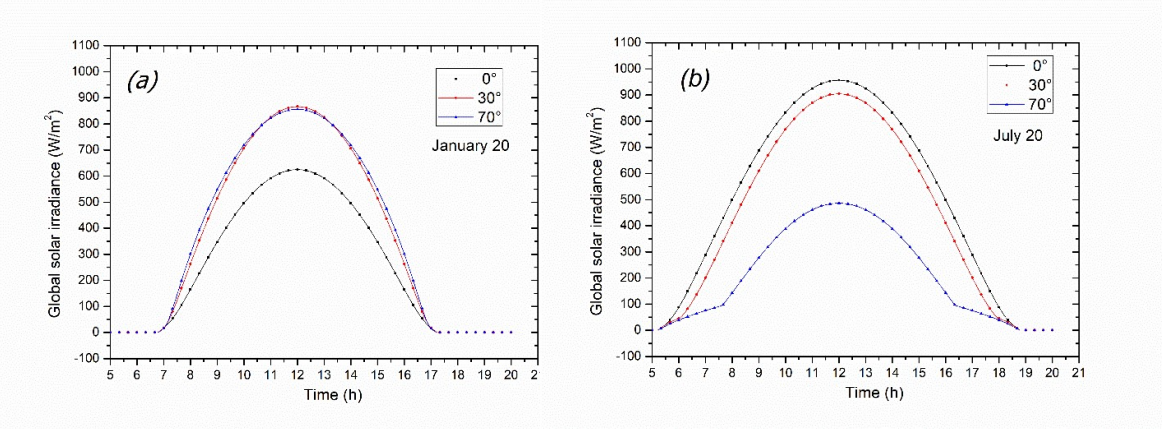


**Figure 5. Temporal variation of simulated global solar irradiance on planes with different inclinations on two selected days: (a) January 20 and (b) July 20**

#### *3.2.2. Temperatures of the collector components*

Fig. 6 and Tab. 3 show that in winter, the simulated maximum temperatures of the collector components (absorber, glass, and hot air) are highest when the collector is tilted at 70°. At a 30° inclination, the temperatures of the components also reach a good value of 77°C, 67°C, 33°C and 33.5°C concerning the horizontal tilt. In summer, the highest temperatures occur when the collector is tilted horizontally (0°), and the temperatures at this angle are nearly identical to those at 30°C. Based on this simulation result, we conclude that the 30° inclination is the best choice for achieving significant efficiency when the collector must be fixed throughout the year. It is worth noting that this inclination

(30°) is near Adrar's latitude (27.9°). In general, this aligns with the findings of many other researchers [30-32].

**Table 3. Simulated maximum temperature values of the different collector components at different inclinations for the two extreme days of winter and summer**

| Tempertures °C (T1 : absorber, T2 : heated air, T3 : glass cover, T4 : ambient air) | | | | | | |
|---|---|---|---|---|---|---|
| | (a) January 20 | | | (b) Julay 20 | | |
| | ***β= 0°*** | ***β= 30°*** | ***β= 70°*** | ***β= 0°*** | ***β= 30°*** | ***β= 70°*** |
| **T1** | 70 | 77 | 88 | 115.5 | 112.5 | 89.5 |
| **T2** | 58 | 68 | 75 | 106.5 | 104 | 84.5 |
| **T3** | 30.5 | 33.5 | 38 | 72.5 | 71 | 62 |
| **T4** | 14 | 14 | 14 | 48 | 48 | 48 |

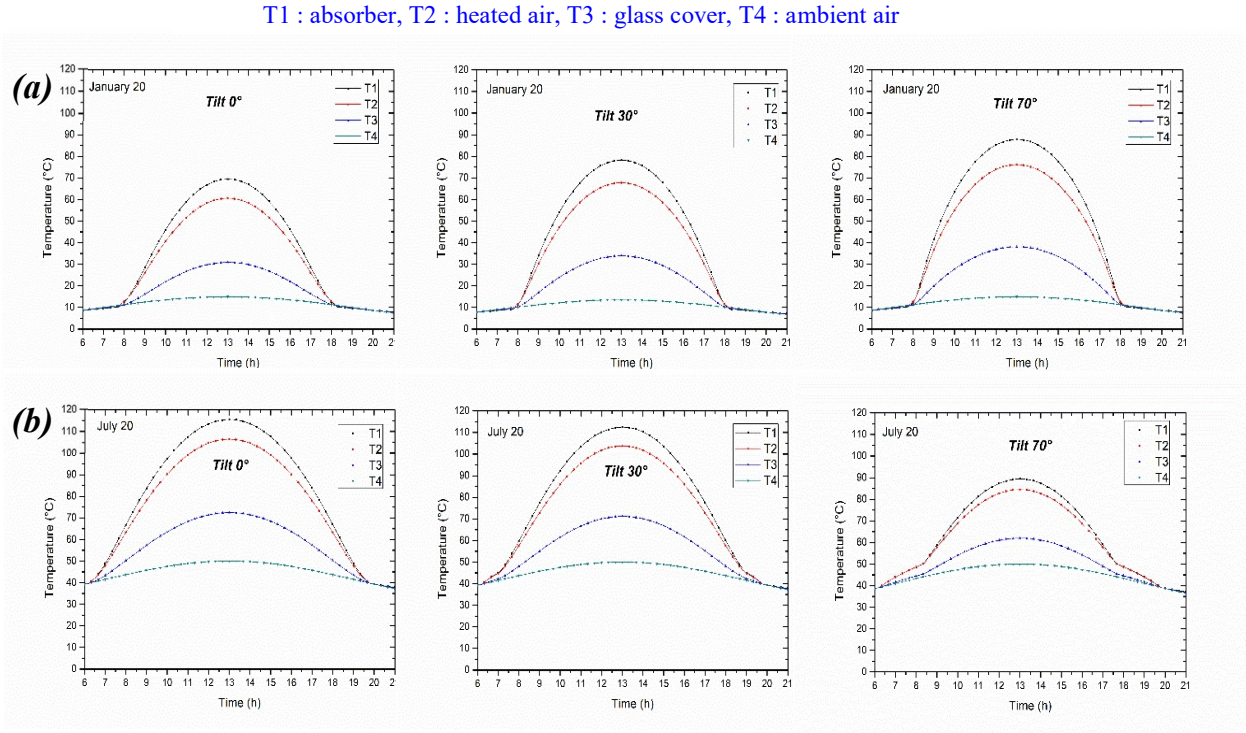


**Figure 6. Temporal variation of simulated temperatures for collector components at different inclination angles for the two days selected: (a) January 20 and (b) July 20**

*3.2.3. Model validations and statistical analysis*

In order to validate our model, we compared the numerical outcomes to the values measured in the URER-MS examination unit to validate our model. According to the curves of Fig. 7 and Fig. 8, the measured and estimated values for the collector's component temperatures are in reasonable accord. Additionally, the measured values of global solar irradiance acquired on an inclined plane extremely conform with the numerical results (Fig. 9).

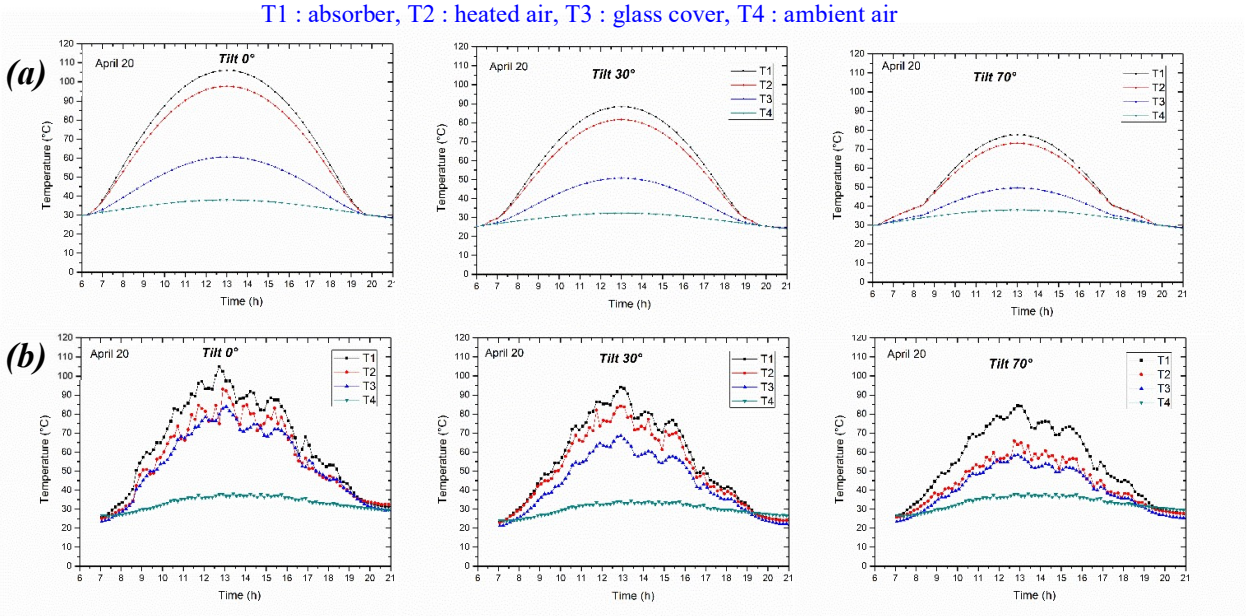


**Figure 7. Temporal variation of temperatures of various collector components at different inclinations on April 20: (a) calculated and (b) measured.**

Tab 4 compares simulated and experimental temperature data for four system components (absorber T1, heated air T2, glass cover T3, and ambient T4) at 0°, 30°, and 70° inclinations. The results indicate that T4 maintains the highest accuracy, with errors ranging from 5.4 to 6.4 %. While T1 and T2 exhibit moderate errors (ranging from 4.8 to 10 % and 5.2 to 14.8 %, respectively), T3 shows the greatest variability, with errors between 10.7 % and 17.3 %. The 30° inclination proves optimal, yielding the lowest deviations for most components. These percentage error ranges confirm the theoretical model's reasonable accuracy in predicting system performance across varying operational conditions.

**Table 4. Absolute and relative temperature errors for: Absorber (T1), Heated air (T2), Glass cover (T3), and Ambient (T4) at different inclination angles**

| Inclination | Error | T1 | T2 | T3 | T4 |
|---|---|---|---|---|---|
| ***0°*** | Absolute Error (°C) | 7 | 7.5 | 8.9 | 1.8 |
| | Relative Error ( %) | 10 | 11.3 | 17.3 | 5.4 |
| ***30°*** | Absolute Error (°C) | 4.5 | 4.9 | 5.2 | 1.7 |
| | Relative Error ( %) | 4.8 | 5.2 | 12.9 | 5.5 |
| ***70°*** | Absolute Error (°C) | 3.2 | 8.1 | 4 | 1.9 |
| | Relative Error ( %) | 6.7 | 14.8 | 10.7 | 6.4 |

The statistical analysis of the experimental data shown in Fig. 7 indicates that the mean values across different temperature conditions (T4, T2(70°), T2(30°), and T2(0°)) are essential for determining the significance of temperature effects. The mean temperature values indicate a progressive increase, suggesting a heat transfer process from the ambient temperature (T4 = 31.23°C) to the heated air temperature (T2 (0°) = 45.36°C). The standard deviation (StDev) values highlight the variability within each parameter, with T4 exhibiting the lowest variability (4.81°C), indicating relatively stable ambient conditions, whereas heated air temperature T2 (30°) shows the highest fluctuation (23.96°C). To quantify the reliability of these estimates, the 95% confidence intervals (CI) provide a range in which the true mean values are expected to lie with 95% certainty. For instance, the confidence interval for T4

(29.53°C – 32.94°C) is relatively narrow, indicating high precision, whereas T2(70°) (35.57°C – 38.89°C) and T2(0°) (43.65°C – 47.07°C) have wider confidence intervals, suggesting greater uncertainty in these temperature measurements. The pooled standard deviation (18.07°C) represents the overall variability across all temperature parameters. Given the relatively high standard deviation for T4, T2(70°), T2(30°), and T2(0°). A one-way ANOVA test could further quantify the significance of the mean differences among the temperature levels. The p-value is less than the chosen significance level (a=0.05). The Margin of Error (ME) at a 95% Confidence Interval (CI) is expected to lie within ± 1.7 °C (or ±1.7 °C for Tamb. The increasing trend suggests that higher temperatures influence the measured parameter significantly with T2(0°) showing the highest mean. The confidence intervals and margin of error highlight measurement uncertainties, suggesting that additional data collection and processing refinement are needed. The calculated margin of error and confidence intervals confirm the reliability of the data, while the standard deviations highlight potential inefficiencies in heat absorption and transfer.

The one-way analysis of variance (ANOVA) results indicate statistical significance at a 95% confidence interval, demonstrating the robustness of the experimental data. These findings also confirm the adequacy and reliability of the experimental design.

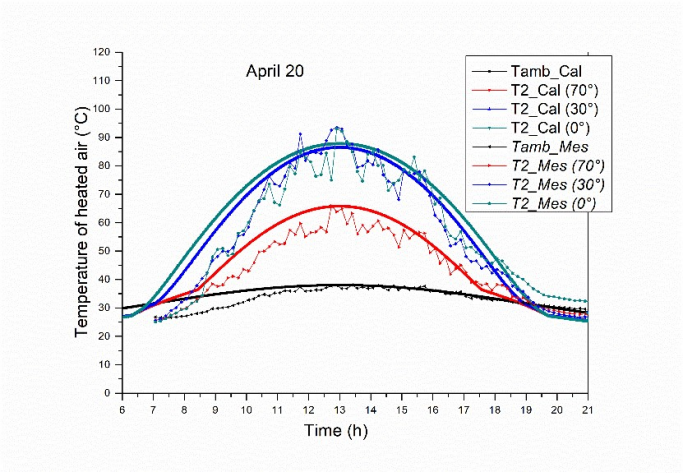


**Figure 8. Temporal variation of the heated air temperature for the collector inclined at 30° on April 20 (calculated and measured)**

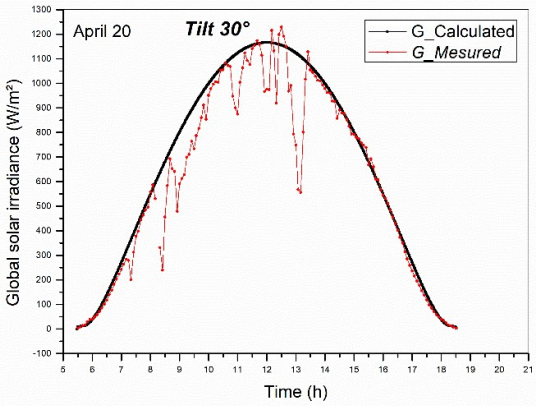


**Figure 9. Temporal variation of global solar irradiance on a surface inclined at 30° on April 20 (calculated and measured)**

## 4. Conclusions

Solar air collectors have been widely utilized in the technology of low-temperature solar energy, such as the drying of agricultural products. Knowing the solar collector parameters helps predict thermal performance under different climatic conditions. The present study consisted of a theoretical and experimental study of a single-pass solar air collector. The theoretical study was based on developing a computer code to solve the energy equations to predict the system's thermal performance. The temperatures of various collector components (absorber, glass cover, and heated air) were studied in different seasons. The inclination angle of the collector affects its performance depending on the season. In winter, the thermal performance of the solar collector improves with increasing the angle, while the opposite occurs in summer. The 30°inclination is suitable for all seasons. At this inclination, the difference between inlet and outlet air temperatures reaches 54 °C, 50 °C, 56 °C, and 53 °C, respectively, for January 20, April 20, July 20, and October 20. The model validation demonstrated percentage deviations between

predicted and experimental values across all inclination angles, with the following ranges: absorber temperature (4.8-10%), heated air temperature (5.2-14.8%), glass cover temperature (10.7-17.3%), and ambient temperature (5.4-6.4%). These results verify that the theoretical model provides acceptably accurate predictions of system performance across different operational conditions. We plan to initiate a simulation and experimental study using our collector in an indirect solar dryer to dry agricultural products, such as tomatoes.

**Acknowledgement**
The Authors also would like to thank Research Unit on Renewable Energies in Saharan Environment (URER-MS) for all the supports**.**

**Nomenclature**

**Symbol**

Cp: specific heat [J $kg^{-1}$ $K^{-1}$]
G: intensity of solar irradiance [W $m^{-2}$]
T: temperture [°C]
t: time [s]
hc: convective transfer coefficient [W $m^{-2}$ $K^{-1}$]
hr: radiative transfer coefficient [W $m^{-2}$ $K^{-1}$]
Ut: top heat loss coefficient [W $m^{-2}$ $K^{-1}$]
Ub: back heat loss coefficient [W $m^{-2}$ $K^{-1}$]
D: hydraulic diameter [m]
L: length of collector [m]
$v_{ext}$: wind speed [m $s^{-1}$]
$\dot{m}_f$: air mass flow rate [kg $s^{-1}$]
w: width of collector [m]
e: thickness [m]

**Subscripts**

a: ambient air
b: absorber plate
f : heated air
i: insulator
v: glasse cover

## References

[1] Swetman, T., Le séchage solaire (Solar drying), Pratical action., Royaume Uni, 2007

[2] Moein Addini, M., Gandjalikhan Nassab, S. A., Numerical simulation of an efficient circular solar air heater integrated with a CPC, *Thermal Science and Engineering Progress*, *56* (2024), Dec., 103092, https://doi.org/10.1016/j.tsep.2024.103092

[3] Tchinda, R. A., *et al.,* Review of the mathematical models for predicting solar air heaters systems, *Renewable and Sustainable Energy Reviews, 13* (2009), 8, pp.1734-1759, https://doi.org/10.1016/j.rser.2009.01.008

[4] Kunwer, R., *et al.,* Thermal Characterization of flat plate solar collector using Titanium Dioxide Nanofluid, *Process Integration and Optimization for Sustainability, 7* (2023), Jun., pp. 1333–1343, https://doi.org/10.1007/s41660-023-00345-8

[5] Salhi, M., *et al.,* Experimental and numerical investigation of the incorporation of an air temperature controller for indirect solar dryers, *Energy Conversion and Management: X, 23* (2024), Jul., 100658, https://doi.org/10.1016/j.ecmx.2024.100658

[6] Yang, M., Experimental analysis on thermal performance of a solar air collector with a single pass, *Build Environ*, *56* (2012), Oct., pp. 361-369, https://doi.org/10.1016/j.buildenv.2012.04.009

[7] Lingayat, A. B., *et al.,* A review on indirect type solar dryers for agricultural crops – Dryer setup, its performance, energy storage and important highlights, *Applied Energy, 258* (2020), 15, 114005, https://doi.org/10.1016/j.rineng.2024.102877

[8] Shekata, G. D., *et al.,* Recent advancements in indirect solar dryer performance and the associated thermal energy storage, *Results in Engineering, 24* (2024), Jan., 102877, https://doi.org/10.1016/j.apenergy.2019.114005

[9] Lingayat, A. *et al.,* Design, Development and performance of indirect Type solar dryer for Banana drying, *Energy Procedia, 109* (2017), pp. 409-416, https://doi.org/10.1016/j.egypro.2017.03.041

[10] Aissa, W., *et al.,* Performance of solar dryer chamber used for convective drying of Sponge-Cotton, *Thermal Science* 18 (2014), 2, pp. S451-S462, https://doi: 10.2298/TSCI110710084A

[11] El-Sebaey, M. S., *et al.,* Proposing novel approach for indirect solar dryer integrated with active-fan and passive-chimney: An experimental and analytical investigation, *Energy, 304* (2024), Sep., 132215, https://doi.org/10.1016/j.energy.2024.132215

[12] Hao, W., *et al.,* Research on operation strategy and performance prediction of flat plate solar collector with dual-function for drying agricultural products, *Renewable Energy, 127* (2018), pp. 685-696, https://doi.org/10.1016/j.renene.2018.05.021

[13] El-Bialy, E., *et al.,* Recent developments and cost analysis of different configurations of the solar air heaters, *Solar Energy, 265* (2023), 15, 112091, https://doi.org/10.1016/j.solener.2023.112091

[14] Aouissi, Z., *et al.,* Numerical and experimental study of thermal efficiency of the transversal rectangular baffles with incline angle inside of solar air collector, *Energy Sources, 44* (2022), 4, pp. 8921-8942, https://doi.org/10.1080/15567036.2022.2128474

[15] Patela, V., *et al.,* Effect of channel depth ratio and absorber plate configuration on performance of a solar air heater, *Case Studies in Thermal Engineering, 61* (2024), Sep., 104789, https://doi.org/10.1016/j.csite.2024.104789

[16] Shreyas P., *et al.,* Numerical analysis of a solar air heater with circular perforated absorber plate, Solar Energy, *215* (2021), Fen., pp. 416-433, https://doi.org/10.1016/j.solener.2020.12.053

[17] Zhang, R., *et al.,* Numerical model and efficiency analysis of finned staggered solar PV/T air collector, *Thermal Science, 28* (2024), 2A, pp. 941-960, https://doi.org/10.2298/TSCI230409179Z

[18] Chabane, F., and Aouissi, Z., Experimental investigations on the thermal efficiency of a solar air collector with transverse rectangular baffles inclined by an angle of 135°, *Energy and Built Environment, 5* (2024), 4, pp. 544-555, https://doi.org/10.1016/j.enbenv.2023.04.004

[19] Romàn, F., and Hensel, O., A comparison of steady-state and transient modelling approaches for the performance prediction of solar air heaters, *Energy Conversion and Management: X* , *16* (2022), Dec., 100327, https://doi.org/10.1016/j.ecmx.2022.100327

[20] Hernández, A., Salvo, N., Evaluación computacional de la eficiencia térmica de colectores calentadores de aire. Estudio paramétrico para dos configuraciones, *Avances en Energías Renovables y Medio Ambiente, 12* (2008), 1, pp. 93-100

[21] Muster, W., Alaiwi, Y., Experimental investigation of thermal performance of single pass solar collector using high porosity metal foams, *Case Studies in Thermal Engineering, 45* (2023), pp. 102879, https://doi.org/10.1016/j.csite.2023.102879

[22] Selmi, M., *et al.,* Validation of CFD simulation for flat plate solar energy collector, *Renewable Energie*, *33* (2008), 3, pp. 383–387, https://doi.org/10.1016/j.renene.2007.02.003

[23] Suresh, M., Drying of mint leaves in forced convection solar dryer, *Thermal Science*, *23* (2019) 6B, pp. 3941-3949, https://doi.org/10.2298/TSCI171230303S

[24] Al-Kayiem, H., Tadahmun A. Y., On the natural convection heat transfer in a rectangular passage solar air heater, *solar energy, 112* (2015), Feb., pp. 310-318, https://doi.org/10.1016/j.solener.2014.11.031

[25] Duffie, J. A., Beckman, W. A., Solar Engineering of thermal processes, 5th Edition, John Wiley & Sons, Inc., Hoboken, New Jersey, USA, 2020.

[26] Njomo, D., Michel Daguenet, M., Sensitivity analysis of thermal performances of flat plate solar air heaters, *Heat Mass Transfer, 42* (2006), pp. 1065-1081, doi: 10.1007/s00231-005-0063-9

[27] Serth, R. W., Lestina T. G., Process Heat Transfer: Principles Principles, Applications and Rules of Thumb, Second edition, Elsevier, Texas, USA, 2014

[28] Daguenet, M., Les séchoirs solaires théorie et pratique (Solar dryers theory and practice). UNESCO, 1985

[29] Modarresi, J., Hosseinnia, H., Worldwide Daily Optimum Tilt Angle Model to Obtain Maximum Solar Energy, IETE JOURNAL OF RESEARCH, (2020), pp. 1-9, https://doi.org/10.1080/03772063.2020.1831412

[30] Benghanem, M., Optimization of tilt angle for solar panel: Case study for Madinah, Saudi Arabia, *Applied Energy, 88* (2011), 4, pp. 1427-1433, https://doi:10.1016/j.apenergy.2010.10.001

[31] El-Kassaby M.M., Monthly and daily optimum tilt angle for south facing solar collectors; theoretical model, experimental and empirical correlations, *Solar Wind Technol, 5* (1988), pp. 589-596, https://doi.org/10.1016/0741-983X(88)90054-9

[32] Calabrò, E., An algorithm to determine the optimum tilt angle of a solar panel from global horizontal solar radiation, *Journal of Renewable Energy*, *1* (2013), pp. 1-12, https://doi.org/10.1155/2013/307547

RECEIVED DATE: 13.02.2025.
DATE OF CORRECTED PAPER: 2.3.2025.
DATE OF ACCEPTED PAPER: 23.4.2025.